STELLAR CONTENTS AND GLOBULAR CLUSTER CANDIDATES IN THE SCULPTOR GROUP GALAXY NGC 300

SANG CHUL KIM, HWANKYUNG SUNG, AND MYUNG GYOON LEE
Astronomy Program, SEES, Seoul National University, Seoul 151-742, Korea
E-mail: sckim@astro.snu.ac.kr, sungh@astro.snu.ac.kr, mglee@astrog.snu.ac.kr

ABSTRACT

We present $UBVI$ CCD photometry of the stellar contents and globular cluster(GC) candidates in the spiral galaxy NGC 300 in the Sculptor group. Color-magnitude diagrams for 18 OB associations having more than 30 member stars are presented. The slope of the initial mass function for the bright stars in NGC 300 is estimated to be $\Gamma = -2.6 \pm 0.3$. Assuming the distance to NGC 300 of $(m - M)_0 = 26.53 \pm 0.07$, the mean absolute magnitude of three brightest blue stars is obtained to be $< M_V^{BSG}(3) > = -8.95$ mag. We have performed search for GCs in NGC 300 and have found 17 GC candidates in this galaxy. Some characteristics of these GC candidates are discussed.

Key words : galaxies: spiral – galaxies: photometry – galaxies: stellar content – galaxies: star clusters – galaxies: individual (NGC 300) – stars: early type – stars: supergiants

I. INTRODUCTION

Sculptor group is the nearest galaxy group to the Local Group containing five major spiral galaxies (NGC 55, NGC 247, NGC 253, NGC 300, and NGC 7793) and ∼20 dwarf galaxies (Côté et al. 1997, Whiting 1999; cf. van den Bergh 1999). Due to the rather small distance to the Sculptor group, there have been many studies on the galaxies in this group.

NGC 300 (=ESO 295-20, IRAS 00523-3756, PGC 3238) is an SA(s)d spiral galaxy in the Sculptor group. Basic information of this galaxy is summarized in Table 1. It is a rather bright ($M_B = -18.6$) and nearly face-on galaxy, similar to M33 seen in the northern hemisphere (Blair & Long 1997). There have been several studies on NGC 300, and some of them are summarized in the following. Pietrzyński et al. (2001) have found 117 OB associations in NGC 300, Davidge (1998) has studied the evolved red stellar contents from JHK photometry, Breysacher et al. (1997) have studied Wolf-Rayet stars detected in five associations of NGC 300, and Soffner et al. (1996) have searched for and found 34 planetary nebulae and 88 H II regions. Freedman et al. (1992) obtained the distance modulus to this galaxy of $(m - M)_0 = 26.66 \pm 0.10$ mag (d = 2.1 ± 0.1 Mpc) using 16 known Cepheid variables. Pannuti et al. (2000) have conducted supernova remnant (SNR) search in NGC 300 using X-ray, optical, and radio observations, resulting in total 44 SNR candidates including 16 new objects. Recently Read & Pietsch (2001) have studied X-ray emission sources in NGC 300 using $ROSAT$ data. Freedman et al. (2001) have revised the distance modulus to NGC 300 using the $Hubble\ Space\ Telescope$ Key Project Cepheid data to be

$(m - M)_0 = 26.53 \pm 0.07$ mag (d = 2.02 ± 0.07 Mpc), which is adopted in this study.

There have been a few surveys for globular clusters(GCs) in the Sculptor group galaxies. From excellent seeing plates and spectrophotometry, Da Costa & Graham (1982) have found three GCs in edge-on galaxy NGC 55. Liller & Alcaino (1983a) have found 51 GC candidates in NGC 55 from excellent-seeing plates taken with ESO 3.6m telescope. Liller & Alcaino (1983b) also have found 63 GC candidates in NGC 253 from excellent-seeing plates taken with ESO 3.6m telescope. In NGC 253, Blecha (1986) have found 25 GC candidates from using high-resolution-wide field McMullan electronographic camera attached to the Danish 1.5m telescope. Later, for the 57 and 58 GC candidates in NGC 55 and NGC 253, respectivey, Beasley & Sharples (2000) have performed spectroscopic GC survey and identified one probable GC and 14 GCs in NGC 55 and NGC 253, respectivey. And they have estimated total number of GCs in NGC 55 and NGC 253 to be ∼20 and ∼60, respectivey. Watson et al. (1996) have discovered four young, luminous, compact stellar clusters in the central region of the starburst spiral galaxy NGC 253, which are believed to be excellent candidates of young GCs. Recently Jerjen & Rejkuba (2001) have found one GC candidate in dwarf galaxy ESO 540-032 using Very Large Telescope UT1+FORS1. However, little is known about GCs in NGC 300. Only Bright & Olsen (2000) have indicated that they obtained 100 – 150 GC candidates in each of seven brightest galaxies in the Sculptor group. But the detailed information is not yet published. In this paper we report the first list of GC candidates in NGC 300.

This paper is composed as follows. Section II describes observations and data reduction, and Section III presents photometric diagrams and photometric anal-

---

Corresponding Author: S. C. Kim

Table 1. Basic Information of NGC 300

Parameter	Information	Reference
α_{2000}, δ_{2000}	$0^h\ 54^m\ 53.^s8$, $-37°\ 40'\ 57''$	de Vaucouleurs et al. 1991
l, b	$29.^°20$, $-79.^°42$	de Vaucouleurs et al. 1991
Type	SA(s)d	de Vaucouleurs et al. 1991
H I heliocentric radial velocity, $v_\odot$	142 ± 4 km s^{-1}	de Vaucouleurs et al. 1991
Maximum rotational velocity, V_m	87 km s^{-1}	Carignan 1985
Foreground reddening, $E(B-V)$	0.013 mag	Schlegel et al. 1998
Isophotal major diameter at the 25.0 B mag arcsec^{-2} level, D_{25}	$21.'9$	de Vaucouleurs et al. 1991
Position angle	$111°$	de Vaucouleurs et al. 1991
Minor to major axis ratio at D_{25}, $(b/a)_{25}$	0.74	Carignan 1985
Inclination i	$42.°3 \pm 3.°0$	Carignan 1985
Distance modulus, $(m-M)_0$	26.53 ± 0.07 mag	Freedman et al. 2001
Distance, d	2.02 ± 0.07 Mpc ($1'' = 9.8$ pc)	Freedman et al. 2001
Exponential disk corrected central surface brightness, $\mu_B(0)$	22.23 mag arcsec^{-2}	Carignan 1985
Scale length, r_s	2.06 kpc	Carignan 1985
Apparent total magnitude, B_T	8.72 ± 0.05 mag	de Vaucouleurs et al. 1991
Apparent total color index, $(B-V)_T$	0.59 ± 0.03 mag	de Vaucouleurs et al. 1991
Apparent total color index, $(U-B)_T$	0.11 ± 0.03 mag	de Vaucouleurs et al. 1991
Corrected total magnitude, B_T^0	8.53	de Vaucouleurs et al. 1991
Corrected total color index, $(B-V)_T^0$	0.56	de Vaucouleurs et al. 1991
Corrected total color index, $(U-B)_T^0$	0.09	de Vaucouleurs et al. 1991
Absolute total magnitude, M_{B_T}	-18.59	Sandage & Tammann 1981
Metallicity from the ratio of carbon stars to M stars of spectral type M5 or later, [Fe/H]	-0.5 dex	Richer, Pritchet, & Crabtree 1985
H I column density in the direction of NGC 300	2.97×10^{20} atoms cm^{-2}	Read, Ponman, & Strickland 1997
H I flux	≤ 670 Jy km s^{-1}	Carignan 1985
H I mass, M_{HI}	$(2.5 \pm 0.1) \times 10^9\ M_\odot$	Rogstad, Crutcher, & Chu 1979

yses of 18 OB associations in NGC 300. Section IV presents the search method and the result for new GC candidates, and Section V discusses mass function of bright stars, brightest stars, some characteristics of GCs, and the nucleus of NGC 300. Finally, a summary and conclusions are given in Section VI.

II. OBSERVATIONS

$UBVI$ CCD photometry was performed on 1997 November 23 at the Siding Spring Observatory with the 40 inch (1m) telescope (f/8) and a thinned SITe 2048×2048 CCD (24μm pixels). The scale was $0.''602$ pixel^{-1}, giving $20.'5$ on a side. Exposure times used in the observations were 60 s and 120 s in I, 300 s in V, 600 s in B, 1200 s in U. The night was photometric and the seeing was $1.''4$ in the 300 sec V image. A finding chart for the observed area is shown in Fig. 1. In the figure we marked only stars with $V = 16.5 - 21$ mag to show the spatial distribution of bright stars in NGC 300. In addition we also marked 18 rich OB associations and 17 GC candidates.

All the preprocessing, such as overscan correction, bias subtraction and flat fielding were done using the IRAF[1]/CCDRED package. Instrumental magnitudes were obtained using the IRAF version of DAOPHOT II (Stetson 1990) via point spread function (PSF) fitting. All the instrumental magnitudes were trans-

formed to the standard Johnson-Cousins $UBVI$ system using SAAO observations of equatorial standards (Menzies et al. 1991) and blue and red standards by Kilkenny et al. (1998). The primary extinction coefficients were determined and used. Details involving standard transformations can be found in Sung & Bessell (2000).

The total number of stars which were measured down to $V = 22$ mag is 6027. Table 2 lists the photometry of 167 stars with $V < 19.0$ mag and contains the running number, α (J2000.0), δ (J2000.0), the weighted mean values of the magnitude and color, the weighted errors, and the number of independent measurements. The variable stars found by Graham (1984), the photometric sequence of Graham (1981) and Walker (1995), and GC candidates newly found in this paper are identified in the last two columns.

The mean values of the errors are listed in Table 3 ("N" in Table 3 represents the number of stars used in the statistics). The $UBVI$ magnitude and colors for $V_{CCD} \leq 20$ mag are compared with previous photoelectric or CCD photometry by Graham (1981) and Walker (1995) in Fig. 2, showing differences in the sense, previous photometry minus our new photometry. Our photometry is consistent with that by Graham (1981) or by Walker (1995) in $B - V$ and $V - I$ ($\Delta(B-V) = +0.008 \pm 0.013$ and $\Delta(V-I) = -0.007 \pm 0.014$), but slightly fainter in V ($\Delta V = -0.025 \pm 0.024$) and redder in $U - B$ ($\Delta(U-B) = -0.042 \pm 0.016$).

---

[1]IRAF is distributed by the National Optical Astronomy Observatories, which are operated by the Association of Universities for Research in Astronomy, Inc.

Table 2. Photometric data of the bright stars with $V < 19.0$ mag in NGC 300[a]

ID	α (J2000)	δ (J2000)	V	$V-I$	$B-V$	$U-B$	ϵ_V	ϵ_{V-I}	ϵ_{B-V}	ϵ_{U-B}	n_{obs}				V/GC[b]	remarks[c]
1	0:54:17.05	-37:46:50.7	13.093	0.697	0.744	0.360	0.030	0.039	0.036	0.019	1	1	1	1		
2	0:55:44.10	-37:41: 5.7	13.295	0.681	0.635	0.061	0.028	0.038	0.030	0.012	1	1	1	1		
3	0:55:26.36	-37:34:28.4	13.421	0.911	0.866	0.613	0.023	0.028	0.024	0.008	1	1	1	1		
4	0:55: 6.44	-37:42:57.8	13.730	0.628	0.599	0.076	0.010	0.013	0.011	0.009	1	1	1	1		
5	0:55:40.64	-37:40: 7.3	13.769	0.692	0.615	0.078	0.011	0.021	0.013	0.011	1	1	1	1		
6	0:55:30.32	-37:33:57.5	14.175	0.934	0.875	0.501	0.014	0.018	0.015	0.009	1	1	1	1		
7	0:55: 3.83	-37:51:19.7	14.216	0.691	0.524	-0.029	0.010	0.016	0.013	0.010	1	1	1	1		G8 = W8
8	0:54:29.49	-37:48:39.8	14.385	1.059	1.010	0.864	0.008	0.013	0.009	0.016	1	1	1	1		
9	0:54:50.90	-37:51:40.7	14.441	0.866	0.880	0.623	0.006	0.013	0.008	0.012	1	1	1	1		G9 = W9
10	0:55:44.43	-37:39:27.3	14.649	0.854	0.819	0.442	0.009	0.020	0.011	0.013	1	1	1	1		
11	0:54:52.63	-37:49: 6.9	14.679	0.973	0.592	0.181	0.008	0.016	0.010	0.010	1	1	1	1		
12	0:54:25.23	-37:35:39.5	15.065	0.914	0.836	0.310	0.008	0.016	0.010	0.011	1	1	1	1		
13	0:55:45.52	-37:40:42.2	15.357	1.039	0.959	0.757	0.012	0.035	0.016	0.018	1	1	1	1		
14	0:54:46.90	-37:41:40.2	15.419	1.122	1.094	0.985	0.006	0.011	0.008	0.019	1	1	1	1		
15	0:54:36.53	-37:34: 9.2	15.427	1.086	1.051	0.898	0.008	0.015	0.011	0.017	1	1	1	1		
16	0:55:39.86	-37:37:25.6	15.506	0.963	0.924	0.722	0.012	0.024	0.014	0.016	1	1	1	1		
17	0:55:35.12	-37:41:54.6	15.597	0.900	0.874	0.628	0.012	0.025	0.014	0.017	1	1	1	1		
18	0:54:49.12	-37:40:12.7	15.634	0.679	0.608	-0.103	0.007	0.012	0.009	0.010	1	1	1	1		
19	0:54:39.50	-37:33:20.0	15.718	0.671	0.591	-0.044	0.009	0.015	0.011	0.013	1	1	1	1		
20	0:55:45.62	-37:40:40.8	15.766	1.212	1.067	0.895	0.013	0.026	0.016	0.024	1	1	1	1		
21	0:55:16.00	-37:37: 8.6	15.819	0.851	0.769	0.274	0.007	0.013	0.009	0.013	1	1	1	1		
22	0:55:44.54	-37:41:15.1	15.884	0.732	0.634	0.117	0.010	0.023	0.011	0.013	1	1	1	1		
23	0:55: 5.68	-37:44:47.1	15.966	1.145	1.078	0.998	0.008	0.013	0.011	0.024	1	1	1	1		
24	0:54:39.53	-37:37:13.8	16.056	0.814	0.751	0.176	0.009	0.016	0.011	0.012	1	1	1	1		
25	0:55:36.78	-37:36:23.6	16.083	0.695	0.625	-0.014	0.009	0.017	0.011	0.014	1	1	1	1		
26	0:54:12.60	-37:49: 3.5	16.097	0.862	0.681	0.122	0.028	0.043	0.034	0.027	1	1	1	1		
27	0:55:32.53	-37:41:20.5	16.142	0.964	0.935	0.715	0.008	0.015	0.010	0.020	1	1	1	1		
28	0:55:50.77	-37:50: 9.2	16.202	1.698	1.383	1.282	0.013	0.021	0.021	0.048	1	1	1	1		
29	0:54:53.41	-37:41: 2.8	16.365	0.939	0.657	0.094	0.047	0.074	0.059	0.047	1	1	1	1		
30	0:54:24.97	-37:44:29.9	16.369	0.726	0.637	-0.015	0.009	0.021	0.012	0.014	1	1	1	1		
31	0:55:19.23	-37:36:35.6	16.423	1.283	1.094	0.998	0.011	0.021	0.013	0.023	1	1	1	1		
32	0:54:22.85	-37:39:31.4	16.451	1.399	1.247	1.131	0.013	0.024	0.017	0.039	1	1	1	1		
33	0:54:48.43	-37:49:51.1	16.590	0.901	0.780	0.321	0.011	0.025	0.014	0.019	1	1	1	1		
34	0:54:21.83	-37:32: 8.4	16.703	0.855	0.757	0.333	0.019	0.031	0.022	0.021	1	1	1	1		
35	0:55: 9.32	-37:33:37.8	16.705	1.443	1.332	1.171	0.008	0.019	0.013	0.060	1	1	1	1		
36	0:54:21.18	-37:38: 3.6	16.746	0.777	0.730	0.047	0.014	0.024	0.017	0.019	1	1	1	1		
37	0:55:12.40	-37:45:54.6	16.795	0.801	0.622	0.073	0.011	0.016	0.014	0.020	1	1	1	1		
38	0:54:26.02	-37:51:59.2	16.852	1.037	0.912	0.653	0.013	0.025	0.016	0.028	1	1	1	1		
39	0:55:35.58	-37:35:41.7	16.973	0.623	0.423	-0.166	0.012	0.021	0.015	0.017	1	1	1	1		
40	0:55:35.13	-37:34:49.0	17.150	0.866	0.676	0.038	0.015	0.030	0.018	0.023	1	1	1	1		
41	0:54:35.03	-37:46:12.4	17.196	0.814	0.675	0.060	0.011	0.022	0.016	0.022	1	1	1	1		
42	0:55:26.02	-37:45:31.2	17.220	1.169	0.988	0.821	0.011	0.019	0.014	0.045	1	1	1	1		
43	0:55:53.09	-37:38:27.6	17.267	0.593	0.415	-0.194	0.016	0.039	0.019	0.025	1	1	1	1		
44	0:54:32.37	-37:39:52.8	17.307	0.676	0.449	-0.225	0.012	0.022	0.015	0.018	1	1	1	1		
45	0:55: 0.96	-37:34:38.2	17.307	2.706	1.560	1.294	0.012	0.025	0.019	0.097	1	1	1	1		
46	0:55:27.02	-37:32:27.6	17.327	1.972	1.378	1.265	0.021	0.027	0.026	0.106	1	1	1	1		
47	0:54:39.67	-37:42:12.8	17.398	0.697	0.576	-0.089	0.010	0.021	0.013	0.023	1	1	1	1		
48	0:54:37.50	-37:46: 2.6	17.504	1.615	1.377	1.350	0.010	0.021	0.020	0.093	1	1	1	1		
49	0:54:53.72	-37:32:24.3	17.509	2.091	1.436	0.972	0.013	0.019	0.018	0.056	1	1	1	1		
50	0:55: 3.65	-37:43:19.2	17.618	-0.272	-0.226	-1.166	0.048	0.082	0.065	0.064	1	1	1	1		
51	0:55:13.54	-37:41:37.4	17.624	-0.026	-0.143	-0.916	0.021	0.035	0.028	0.055	1	1	1	1		
52	0:55:12.22	-37:41:19.2	17.625	· · ·	-0.232	-0.850	0.042	· · ·	0.053	0.059	1	0	1	1		
53	0:55:54.93	-37:43:32.3	17.627	1.292	1.144	1.041	0.018	0.032	0.027	0.077	1	1	1	1		
54	0:54:30.27	-37:37:55.5	17.668	0.165	0.089	-0.556	0.012	0.026	0.015	0.015	1	1	1	1		
55	0:55:30.72	-37:45:43.0	17.674	1.200	1.031	0.846	0.013	0.024	0.017	0.051	1	1	1	1		
56	0:54:52.60	-37:41:48.2	17.678	1.898	1.426	1.216	0.012	0.021	0.018	0.129	1	1	1	1		
57	0:54:50.99	-37:52: 2.9	17.689	1.307	1.123	1.052	0.012	0.019	0.018	0.065	1	1	1	1		W29
58	0:55: 1.00	-37:34:39.9	17.702	2.900	1.575	1.026	0.013	0.021	0.025	0.115	1	1	1	1		
59	0:54:42.79	-37:43: 0.9	17.856	-0.215	-0.020	-1.080	0.041	0.079	0.048	0.045	1	1	1	1		
60	0:54:35.80	-37:43: 5.6	17.878	0.769	0.561	-0.156	0.034	0.046	0.056	0.055	1	1	1	1	g2	
61	0:54:13.22	-37:34:19.3	17.880	0.686	0.555	0.100	0.023	0.037	0.030	0.090	1	1	1	1		
62	0:55:13.74	-37:41:39.5	17.886	0.390	0.317	-0.333	0.023	0.040	0.044	0.053	1	1	1	1		
63	0:55:20.28	-37:48: 7.1	17.927	3.081	1.684	1.301	0.013	0.018	0.025	0.157	1	1	1	1		
64	0:55:51.13	-37:37: 3.6	17.954	1.556	1.296	0.815	0.017	0.031	0.025	0.111	1	1	1	1		
65	0:54:42.77	-37:40: 3.1	17.984	0.197	0.011	-1.084	0.022	0.036	0.030	0.033	1	1	1	1		
66	0:54:22.97	-37:34:51.3	18.016	0.120	0.051	-0.496	0.024	0.042	0.031	0.028	1	1	1	1		
67	0:55:13.77	-37:37:49.1	18.025	0.362	0.065	-0.943	0.016	0.032	0.018	0.015	1	1	1	1		
68	0:54:40.32	-37:40:53.9	18.027	0.063	-0.118	-1.080	0.040	0.059	0.049	0.052	1	1	1	1		
69	0:54:20.27	-37:34: 2.6	18.060	1.022	0.968	0.668	0.043	0.195	0.051	0.191	1	1	1	1		
70	0:54:21.92	-37:38:14.0	18.091	0.139	0.084	-0.693	0.013	0.041	0.019	0.022	1	1	1	1		
71	0:55:49.97	-37:33:18.3	18.103	0.915	0.589	0.049	0.055	0.080	0.082	0.073	1	1	1	1		
72	0:55:11.03	-37:36:46.1	18.158	1.308	0.601	0.321	0.108	0.122	0.119	0.074	1	1	1	1	g1	
73	0:55:12.91	-37:41:37.9	18.192	-0.135	-0.140	-1.011	0.043	0.061	0.059	0.057	1	1	1	1		
74	0:55: 2.56	-37:38:29.1	18.193	0.213	0.126	-0.192	0.015	0.044	0.022	0.036	1	1	1	1		
75	0:55:35.60	-37:39:34.6	18.193	0.688	0.483	-0.210	0.015	0.035	0.019	0.037	1	1	1	1		
76	0:54:51.57	-37:39:21.0	18.194	1.266	1.018	0.704	0.015	0.023	0.025	0.078	1	1	1	1		
77	0:54:53.10	-37:32:49.5	18.208	1.056	0.945	0.756	0.011	0.022	0.019	0.079	1	1	1	1		
78	0:54:49.85	-37:40:10.5	18.224	0.720	0.665	0.222	0.018	0.031	0.028	0.061	1	1	1	1		
79	0:55: 0.83	-37:46:59.0	18.290	0.866	0.686	0.147	0.015	0.033	0.021	0.053	1	1	1	1		
80	0:54:39.40	-37:38:47.5	18.301	0.296	0.113	-0.482	0.013	0.032	0.021	0.024	1	1	1	1		
81	0:54:25.42	-37:39: 8.5	18.302	0.301	-0.029	-0.804	0.032	0.043	0.040	0.039	1	1	1	1		
82	0:54:12.69	-37:52:19.0	18.324	0.788	0.723	0.123	0.031	0.052	0.040	0.057	1	1	1	1		
83	0:55:12.61	-37:41:39.2	18.328	-0.270	-0.076	-1.234	0.079	0.136	0.132	0.135	1	1	1	1		
84	0:55:24.96	-37:50:56.1	18.360	0.718	0.590	0.042	0.016	0.030	0.021	0.051	1	1	1	1		

Table 2. - Continued

ID	α (J2000)	δ (J2000)	V	$V-I$	$B-V$	$U-B$	ϵ_V	ϵ_{V-I}	ϵ_{B-V}	ϵ_{U-B}	n_{obs}				V/GC[b]	remarks[c]
85	0:54:30.89	-37:49:26.3	18.390	0.793	0.603	-0.079	0.013	0.034	0.023	0.036	1	1	1	1		
86	0:55:12.68	-37:41:39.4	18.393	-0.106	-0.213	-1.081	0.085	0.139	0.133	0.118	1	1	1	1		
87	0:54:26.68	-37:44: 3.5	18.396	0.087	0.097	-0.453	0.016	0.035	0.021	0.028	1	1	1	1		
88	0:55:38.35	-37:41:57.7	18.398	0.238	0.098	-0.719	0.020	0.028	0.024	0.022	1	1	1	1		
89	0:54:50.26	-37:38:23.1	18.405	-0.262	-0.140	-0.939	0.040	0.082	0.052	0.060	1	1	1	1		
90	0:55:39.42	-37:43:22.3	18.409	0.817	0.581	-0.035	0.016	0.037	0.034	0.045	1	1	1	1		
91	0:54:17.18	-37:48: 7.5	18.416	0.641	0.432	-0.197	0.019	0.032	0.024	0.030	1	1	1	1		
92	0:54:58.25	-37:41:13.1	18.418	0.890	0.702	0.170	0.016	0.026	0.021	0.046	1	1	1	1		
93	0:55:12.45	-37:41:19.5	18.433	-0.010	-0.071	-0.889	0.021	0.041	0.025	0.027	1	1	1	1		
94	0:54:25.48	-37:39:36.3	18.437	-0.070	-0.052	-0.572	0.028	0.047	0.038	0.049	1	1	1	1		
95	0:54:30.01	-37:50: 5.0	18.441	1.366	1.596	0.495	0.074	0.108	0.105	0.147	1	1	1	1		
96	0:54:14.54	-37:31:53.3	18.451	1.067	0.930	0.585	0.040	0.053	0.080	0.120	1	1	1	1		
97	0:54:42.60	-37:40: 2.9	18.469	0.011	-0.089	-0.981	0.030	0.057	0.041	0.038	1	1	1	1		
98	0:55:29.50	-37:36:43.1	18.492	2.207	1.523	$\cdots$	0.012	0.022	0.021	$\cdots$	1	1	1	0		
99	0:55: 2.38	-37:38:26.8	18.497	-0.157	-0.178	-1.040	0.032	0.059	0.047	0.051	1	1	1	1		
100	0:54:42.69	-37:42:57.8	18.518	1.395	0.308	-0.920	0.055	0.061	0.063	0.055	1	1	1	1		
101	0:54:49.92	-37:40:24.7	18.523	0.575	0.480	0.103	0.021	0.036	0.026	0.052	1	1	1	1		
102	0:54:43.37	-37:36:26.5	18.530	0.100	0.090	-0.579	0.015	0.035	0.021	0.024	1	1	1	1		
103	0:54:54.61	-37:45:46.7	18.552	0.201	0.019	-0.809	0.015	0.036	0.019	0.023	1	1	1	1		
104	0:55:13.16	-37:41:43.2	18.554	0.360	0.088	-0.891	0.024	0.047	0.034	0.041	1	1	1	1		
105	0:54:32.07	-37:37:49.7	18.564	0.186	0.044	-0.813	0.015	0.039	0.019	0.024	1	1	1	1		
106	0:55:14.73	-37:38: 7.0	18.565	1.517	1.259	1.317	0.015	0.022	0.029	0.148	1	1	1	1		
107	0:54:25.51	-37:39:55.1	18.586	1.399	1.242	-0.276	0.029	0.035	0.070	0.095	1	1	1	1		
108	0:55: 3.73	-37:42:51.2	18.606	-0.105	-0.146	-1.019	0.028	0.056	0.037	0.042	1	1	1	1		
109	0:55: 0.90	-37:39:30.2	18.615	0.538	0.347	0.298	0.022	0.045	0.027	0.056	1	1	1	1		
110	0:55:12.07	-37:41:25.2	18.615	-0.268	-0.096	-0.818	0.037	0.080	0.048	0.043	1	1	1	1		
111	0:54:32.47	-37:43:37.2	18.616	0.275	0.173	-0.422	0.017	0.045	0.034	0.040	1	1	1	1		
112	0:54:48.71	-37:44: 3.2	18.624	0.907	0.746	0.209	0.018	0.035	0.026	0.075	1	1	1	1		
113	0:55:13.97	-37:41:42.6	18.629	0.667	-0.193	-0.915	0.034	0.047	0.043	0.041	1	1	1	1		
114	0:54:56.90	-37:41:33.3	18.637	-0.115	-0.081	-0.895	0.022	0.056	0.028	0.025	1	1	1	1		
115	0:54:16.03	-37:35:36.2	18.641	0.965	0.745	0.235	0.046	0.064	0.060	0.078	1	1	1	1		
116	0:54:49.68	-37:38:37.1	18.646	0.426	-0.126	-0.953	0.026	0.048	0.040	0.043	1	1	1	1		
117	0:54:52.99	-37:41:57.9	18.647	0.770	0.505	-0.221	0.019	0.036	0.024	0.037	1	1	1	1		
118	0:54:47.07	-37:40:14.6	18.653	0.901	0.456	-0.453	0.025	0.041	0.033	0.047	1	1	1	1		
119	0:54:59.72	-37:36:49.8	18.654	0.851	0.721	-0.120	0.021	0.033	0.027	0.062	1	1	1	1		
120	0:55: 5.82	-37:41: 5.8	18.692	0.672	0.716	0.301	0.021	0.034	0.030	0.083	1	1	1	1		
121	0:54:57.41	-37:33:55.3	18.705	1.173	1.116	0.348	0.077	0.101	0.101	0.113	1	1	1	1	g2	
122	0:54:44.10	-37:51:54.1	18.710	1.249	1.315	0.406	0.067	0.103	0.099	0.136	1	1	1	1		
123	0:54:55.99	-37:41:11.6	18.712	0.031	-0.102	-0.816	0.022	0.059	0.028	0.029	1	1	1	1		
124	0:54:20.83	-37:38:48.9	18.712	0.617	0.471	0.147	0.020	0.036	0.028	0.050	1	1	1	1		
125	0:55:53.06	-37:45:13.3	18.713	1.136	0.963	0.565	0.017	0.033	0.029	0.086	1	1	1	1		
126	0:55:42.39	-37:34:59.1	18.715	1.747	1.274	0.848	0.015	0.033	0.028	0.200	1	1	1	1		
127	0:54:40.16	-37:39:25.9	18.718	0.238	0.027	-0.485	0.018	0.045	0.022	0.030	1	1	1	1		
128	0:54:20.29	-37:34: 1.9	18.725	0.800	2.333	-0.846	0.108	0.180	0.198	0.383	1	1	1	1		
129	0:54:18.34	-37:35: 2.8	18.727	1.636	1.326	-0.365	0.020	0.034	0.039	0.086	1	1	1	1		
130	0:54:22.44	-37:43:12.4	18.728	1.968	1.383	$\cdots$	0.019	0.025	0.031	$\cdots$	1	1	1	0		
131	0:55:32.41	-37:34:18.7	18.736	-0.281	-0.247	-0.994	0.021	0.061	0.024	0.022	1	1	1	1		
132	0:54:42.84	-37:42:59.7	18.743	-0.055	-0.255	0.110	0.055	0.110	0.081	0.145	1	1	1	1		
133	0:54:45.62	-37:40:16.7	18.751	0.062	0.061	-0.570	0.022	0.060	0.027	0.031	1	1	1	1		
134	0:55:12.23	-37:41:20.9	18.752	-0.054	-0.141	-1.058	0.062	0.098	0.086	0.134	1	1	1	1		
135	0:55:12.24	-37:41:20.3	18.754	0.895	0.070	-0.942	0.104	0.131	0.148	0.112	1	1	1	1		
136	0:55:20.80	-37:48:11.2	18.755	3.187	1.642	$\cdots$	0.018	0.024	0.035	$\cdots$	1	1	1	0		
137	0:54:53.71	-37:41: 1.1	18.756	0.072	0.050	-0.532	0.030	0.081	0.036	0.033	1	1	1	1		
138	0:55: 3.83	-37:43:18.2	18.764	-0.195	-0.185	-0.894	0.080	0.142	0.102	0.093	1	1	1	1		
139	0:55: 4.75	-37:34: 9.2	18.769	1.600	1.424	0.771	0.014	0.022	0.030	0.176	1	1	1	1		
140	0:54:53.35	-37:39: 1.2	18.800	0.337	0.125	-0.516	0.022	0.048	0.026	0.034	1	1	1	1		
141	0:55:22.72	-37:33:40.1	18.803	0.020	-0.094	-0.903	0.023	0.061	0.026	0.026	1	1	1	1		
142	0:54:55.86	-37:40:14.3	18.808	-0.148	-0.195	-0.952	0.037	0.063	0.045	0.036	1	1	1	1		
143	0:54:34.66	-37:37:22.9	18.810	0.382	0.109	-0.225	0.063	0.112	0.082	0.081	1	1	1	1		
144	0:54:28.23	-37:37:54.5	18.833	1.504	1.725	$\cdots$	0.017	0.028	0.039	$\cdots$	1	1	1	0		
145	0:55:24.77	-37:39:34.4	18.835	-0.260	-0.195	-1.103	0.051	0.084	0.070	0.061	1	1	1	1		
146	0:55:13.13	-37:41:39.4	18.836	-0.999	-0.240	-0.998	0.064	0.229	0.085	0.074	1	1	1	1		
147	0:54:45.62	-37:43:41.0	18.839	0.973	0.755	0.197	0.044	0.064	0.059	0.084	1	1	1	1	g2	
148	0:54:50.40	-37:40: 3.6	18.842	0.082	0.074	-0.647	0.039	0.186	0.072	0.094	1	1	1	1		
149	0:55:27.93	-37:44:19.4	18.844	0.667	0.191	-0.977	0.017	0.038	0.024	0.025	1	1	1	1		
150	0:54:43.44	-37:45:32.6	18.861	0.487	0.322	-0.055	0.066	0.078	0.071	0.107	1	1	1	1		
151	0:54:43.43	-37:43: 8.8	18.872	0.037	0.511	-2.105	0.079	0.127	0.151	0.165	1	1	1	1		
152	0:55:24.24	-37:37:28.3	18.873	1.012	0.848	0.226	0.020	0.039	0.030	0.078	1	1	1	1		
153	0:55:38.79	-37:46:30.7	18.884	1.206	1.074	0.267	0.091	0.137	0.122	0.133	1	1	1	1	g3	
154	0:54:57.44	-37:44: 6.4	18.894	0.100	-0.036	-0.693	0.024	0.049	0.036	0.036	1	1	1	1		
155	0:54:40.03	-37:45:46.5	18.894	1.153	0.978	1.152	0.018	0.035	0.032	0.167	1	1	1	1		
156	0:55:12.76	-37:41:41.4	18.896	-0.234	-0.100	-1.017	0.078	0.124	0.105	0.121	1	1	1	1		
157	0:55:27.56	-37:46: 9.4	18.905	1.213	1.065	0.723	0.085	0.136	0.123	0.178	1	1	1	1	g3	
158	0:54:26.13	-37:43:56.9	18.921	0.132	0.090	-0.500	0.020	0.053	0.025	0.023	1	1	1	1		
159	0:55: 3.87	-37:42:50.5	18.944	-0.150	-0.202	-0.932	0.033	0.064	0.044	0.046	1	1	1	1		
160	0:54:44.75	-37:42:39.0	18.950	0.124	-0.059	-1.034	0.017	0.057	0.024	0.025	1	1	1	1		
161	0:55:17.61	-37:38:33.3	18.953	1.585	1.316	$\cdots$	0.021	0.032	0.034	$\cdots$	1	1	1	0		
162	0:55:12.69	-37:41:38.2	18.963	-0.195	-0.375	-0.811	0.099	0.159	0.162	0.154	1	1	1	1		
163	0:55:30.54	-37:40:27.9	18.965	1.328	1.122	0.581	0.094	0.140	0.127	0.133	1	1	1	1		
164	0:54:41.79	-37:38:35.8	18.977	0.249	0.008	-0.956	0.033	0.148	0.039	0.040	1	1	1	1		
165	0:55:36.73	-37:44: 3.9	18.983	2.553	1.413	$\cdots$	0.021	0.028	0.044	$\cdots$	1	1	1	0		
166	0:55:34.45	-37:41:24.7	18.986	1.238	1.028	0.820	0.023	0.038	0.033	0.174	1	1	1	1		
167	0:55:31.98	-37:41:39.1	18.992	-0.059	0.107	-0.341	0.020	0.065	0.031	0.038	1	1	1	1		

[a] Units of right ascension are hours, minutes, and seconds, and units of declination are degrees, arcminutes, and arcseconds.

[b] V: variable star from Graham (1984), GC(g#): GC candidate with its class (#: 1-3 from higher probability to lower probability)

[c] G: Graham (1981); W: Walker (1995)

Fig. 1.— Finding chart for the stars measured from this observation (20.′5 × 20.′5). To show the distribution of bright stars in NGC 300, we plotted only stars with $V = 16.5 - 21$ mag. The size of the dot is proportional to the magnitude of the star. Open circles represent rich OB associations ($N_* \geq 30$) in NGC 300 listed in Pietrzyński et al. (2001). Thin circles are OB associations with $30 \leq N_* < 50$ and thick circles are those with $N \geq 50$. The star symbols indicate the positions of GC candidates (see Section IV).

III. PHOTOMETRIC DIAGRAMS AND OB ASSOCIATIONS

(a) Photometric Diagrams

As NGC 300 is a member of Sculptor group of galaxies ($d \approx 2.02$ Mpc : Freedman et al. 2001), the stars in the galaxy are very faint. In addition many bright blue stars are members of OB associations, and therefore their photometric values contain inevitably large errors due to crowding effect even though we paid much attention to the photometry. The resulting color-magnitude diagrams (CMDs) from our photometry are presented in Fig. 3. In the figure we marked the GC candidates (open circle with dot; see Section IV for the selection criteria) and variable stars found by Graham (1984) (open square with dot). Among 34 variable stars, 22 were identified from the coordinates and charts given by Graham (1984) (The coordiantes given by him are not accurate enough to identify the variables unambiguously). Among the remaining 12 stars, 9 stars are outside our field of view, 3 stars are too faint to be measured from our images.

The $(V, V - I)$ diagram (Fig. 3 (a)) do not give much information on the photometric characteristics of the stars in NGC 300 due partly to the short exposures of I images and partly to the characteristic nature of $V - I$ color, which is insensitive to the temperature variation of blue stars. On the other hand, $U - B$ is rather sensitive to the temperature variation of hot stars, but the blue stars in NGC 300 are very faint in U pass band. Therefore the $(V, U - B)$ CMD also does not give much information on the faint stars. Among the three CMDs, the $(V, B - V)$ diagram shows well-defined blue stars more clearly. We will use only the $(V, B - V)$ diagram in the analysis of the photometric characteristics of stars in NGC 300. In this figure, a large number of faint blue stars can easily be found. They are bona fide members of NGC 300. Apparently stars brighter than $V = 17.5$ mag seem to be foreground thick disk or halo stars in our Galaxy.

We presented the $(U - B, B - V)$ diagram in Fig. 4. As the most bright blue stars are suspected to be blue supergiants in NGC 300, we drew the intrinsic relation for supergiants (Sung 1995) in the figure. Even though
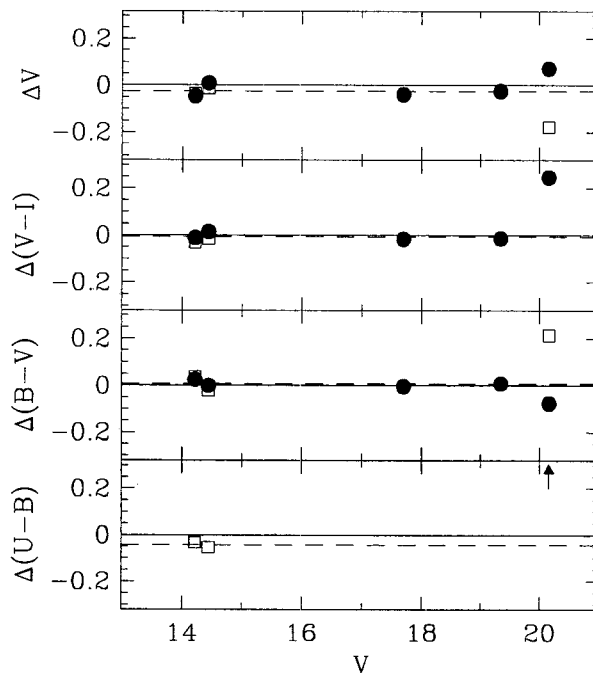
Fig. 2.— Comparison of our photometry with that of Graham (1981) (filled circle) and with that of Walker (1995) (open square), showing differences in the sense, previous photometry minus our new photometry. The arrow symbol in the $\Delta(U - B)$ plot denotes a value well outside of the plot.

the photometric error in $B - V$ as well as $U - B$ is large, most blue stars are scattered around the intrinsic relation for supergiants, indicating that the internal reddening is very small. There are several yellow stars ($B - V = 0.4 - 0.8$ mag). A few of them are GC candidates, but the remainings are foreground stars in the Galaxy. As they are suspected as thick disk or halo stars in the Galaxy, they show evident UV excesses. The others with abnormal red colors in the diagram are faint red stars. Many of them ($V < 17.5$ mag) are foreground red stars in the galaxy, but a few faint red stars may be red supergiant stars in NGC 300. Their abnormal colors are mainly due to large photometric errors. As NGC 300 is located near the south galactic pole ($b = -79.°42$), the foreground reddening due to the interstellar cloud in the Galaxy is practically zero. In addition NGC 300 is nearly face-on, and therefore the internal reddening may not be very large. For the reddening correction of stars in NGC 300 we have used the value $E(B - V) = 0.013$ mag obtained by Schlegel, Finkbeiner, & Davis (1998).

(b)   OB Associations

Recently Pietrzyński et al. (2001) published a catalog of OB associations in NGC 300. They found 117 OB associations using Path Linkage Criterion technique. The telescope they used is the ESO/MPI 2.2 m, and therefore the limiting magnitude of their photometry is about 1 mag fainter than ours. To derive the age distribution of OB associations in NGC 300, the OB

associations having more than 10 stars in our photometry were selected. In the analysis, we limited our attention to the OB associations having more than 30 member stars in the catalog ($N_* > 30$). Among 117 OB associations, 18 OB associations are satisfied the above criterion. We present 18 CMDs with appropriate isochrones of the Padova group (Bertelli et al. 1994) in Fig. 5. Due to the large photometric errors of faint stars in NGC 300, the CMD of individual OB association shows a large scatter. The color of faint stars are more affected by crowding effect (see Sung et al. (1999) for the effect of crowding on color). The large scatter in $B - V$ is therefore due partly to the crowding effect and partly to the contamination of faint field stars in NGC 300. In addition we cannot exclude the possibility of the contamination of foreground stars in the Galaxy or GCs in NGC 300 among yellow or red stars in the line of sight. We determined the age of each association by paying more attention to the bright blue stars in the association.

To obtain the reliable ages of OB associations or young open clusters, spectral type and luminosity class should be known because the photometric indices such as $B - V$ or even $U - B$ are inadequate for the accurate estimate of temperature of O- and early B-type stars. Actually no information on the spectral type of blue stars in NGC 300 is available currently. The ages of OB associations in NGC 300 have, therefore, inevitably large errors if we determine the age from photometric colors alone. We should determine the age of each OB
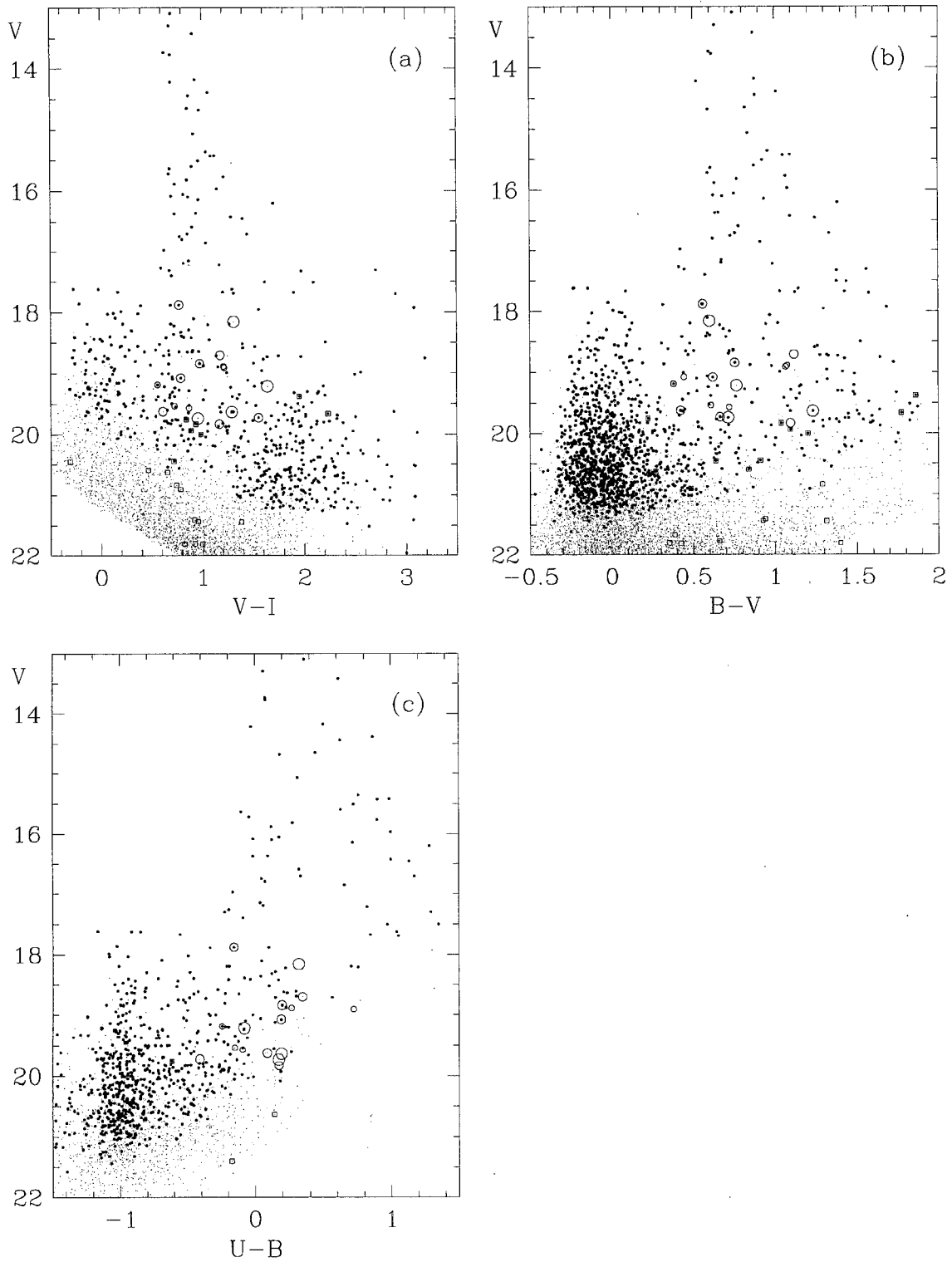
Fig. 3.— Color-magnitude diagrams. Large and small dots represent, respectively, stars with good photometry ($\epsilon \leq 0.1$) and bad quality ($\epsilon > 0.1$). The open squares with dots and open circles with dots denote the known variable stars (Graham 1984) and the GC candidates, respectively. The size of the circle is propotional to the probability of GC in the sense that larger for higher probability, smaller for lower.

Table 3. Mean photometric errors

V	ϵ_V	N	ϵ_{V-I}	N	ϵ_{B-V}	N	ϵ_{U-B}	N
13.5	0.020	5	0.028	5	0.023	5	0.012	5
14.5	0.009	6	0.016	6	0.011	6	0.012	6
15.5	0.009	12	0.019	12	0.012	12	0.016	12
16.5	0.015	16	0.026	16	0.019	16	0.027	16
17.5	0.019	26	0.032	25	0.027	26	0.065	26
18.5	0.035	102	0.065	102	0.051	102	0.074	96
19.5	0.050	370	0.107	357	0.074	369	0.090	312
20.5	0.076	1381	0.178	1190	0.112	1367	0.123	966
21.5	0.128	4175	0.238	2304	0.182	3880	0.152	872
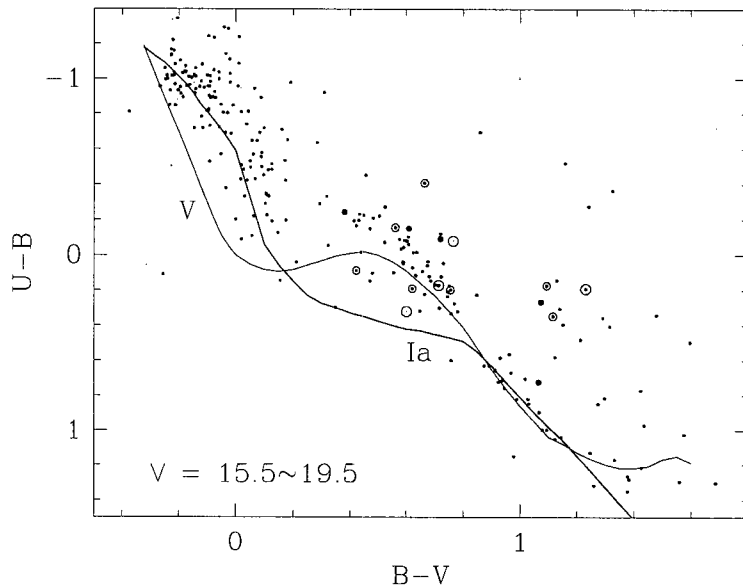
Fig. 4.— $U - B$ versus $B - V$ diagram for $V = 15.5 - 19.5$ mag. The thin and thick solid lines represent the intrinsic zero-age main sequence (ZAMS) relation and the intrinsic relation for supergiants (Ia), respectively. Large and small dots represent, respectively, stars with good photometry ($\epsilon \leq 0.1$) and bad quality ($\epsilon > 0.1$). The open circles with dots at center denote the GC candidates. The size of the circle is propotional to the probability of GC in the sense that larger for higher probability, smaller for lower.

association with such a limitation. Among the 18 OB associations, 13 associations have ages younger than 10 Myr ($\log \tau < 7$). Many of them may have much younger ages (only about a few Myr) because there are a few very bright blue stars ($M_V < -8$ mag). The associations that belong to this category are AS_016, _029, _052, _082, _084, _086, and _102. For these associations the ages from the CMDs are highly uncertain. There are five associations (AS_018, _026, _027, _058, and _096) with ages older than 10 Myr. They have apparently no O-type stars and seem to be old B associations. A few OB associations seem to contain a red supergiant candidate (AS_002, _009, and less luminous red supergiant candidates in AS_101). ·

Spatially these rich OB associations ($N_* > 30$) are more concentrated in the NW part of the galaxy, but

the brightest OB association in NGC 300 is AS_102, about 4′ E of the center of NGC 300. Two out of three brightest blue stars in NGC 300 are in this association. In the Hα image of NGC 300, AS_102 is the brightest in Hα, which indicates that AS_102 is associated with the brightest H II region. AS_102 is the most active star forming region in NGC 300. There are many bright blue stars in the CMD of AS_102. Even though the photometric error is large, there is few red supergiant candiates in the association. This fact again implies that the association is extremely young. The second and third brightest OB associations are AS_052 and _084. Even though AS_052 is the richest OB association ($N_* = 101$) in NGC 300, the brightest star in the associaton is about 0.8 mag fainter that the brightest star in AS_102.
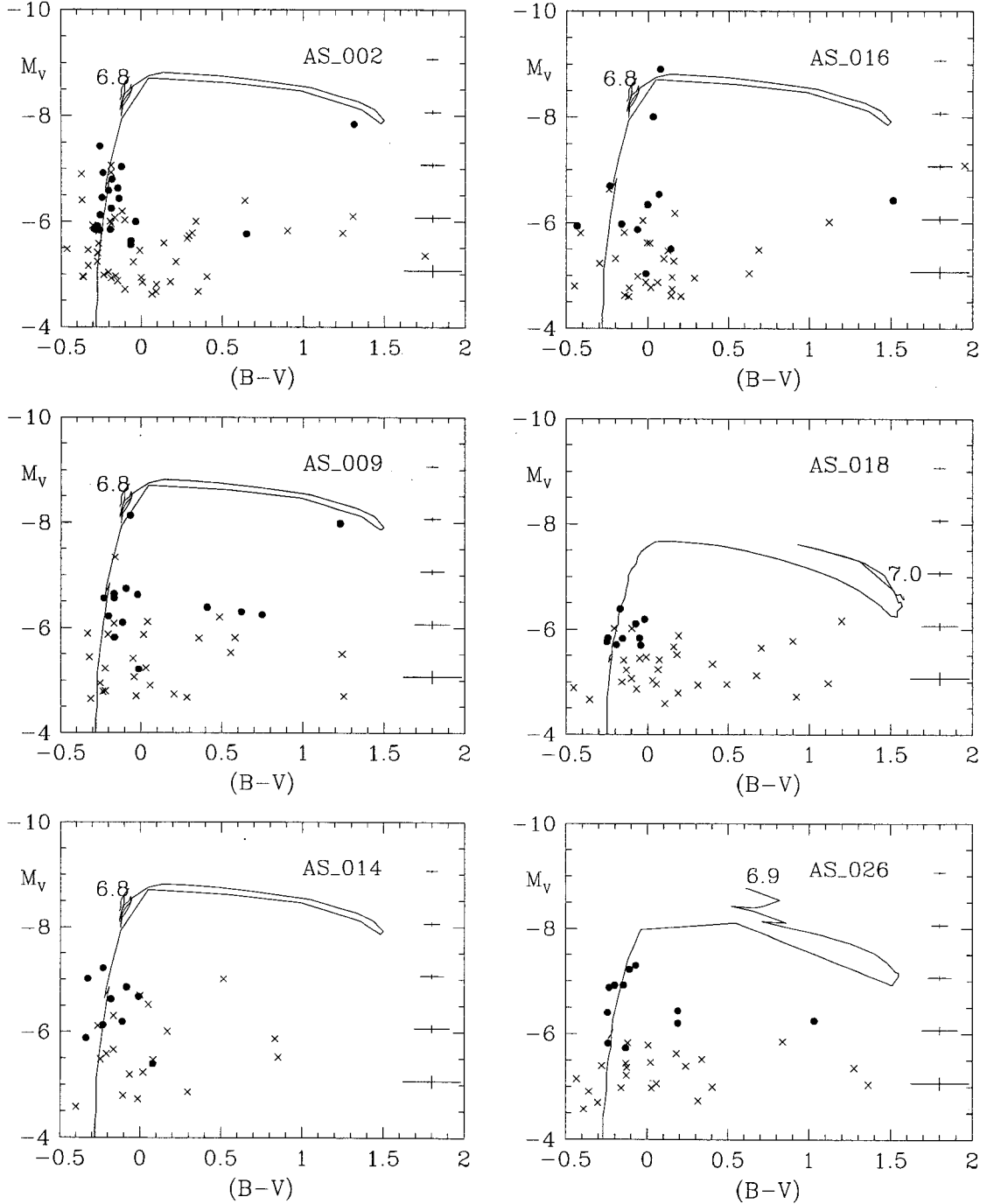
Fig. 5.— Color-magnitude diagrams of selected OB associations. The designation of OB associations is from Pietrzyński et al. (2001). The dot and cross denote, respectively, a star with good photometry ($\epsilon \leq 0.1$) and bad quality ($\epsilon > 0.1$). The mean photometric error in V and $B - V$ is marked in the right part of each diagram. The solid lines represent the isochrones from Bertelli et al. (1994) with the age of the association in a logarithmic scale ($\log \tau_{age}$).
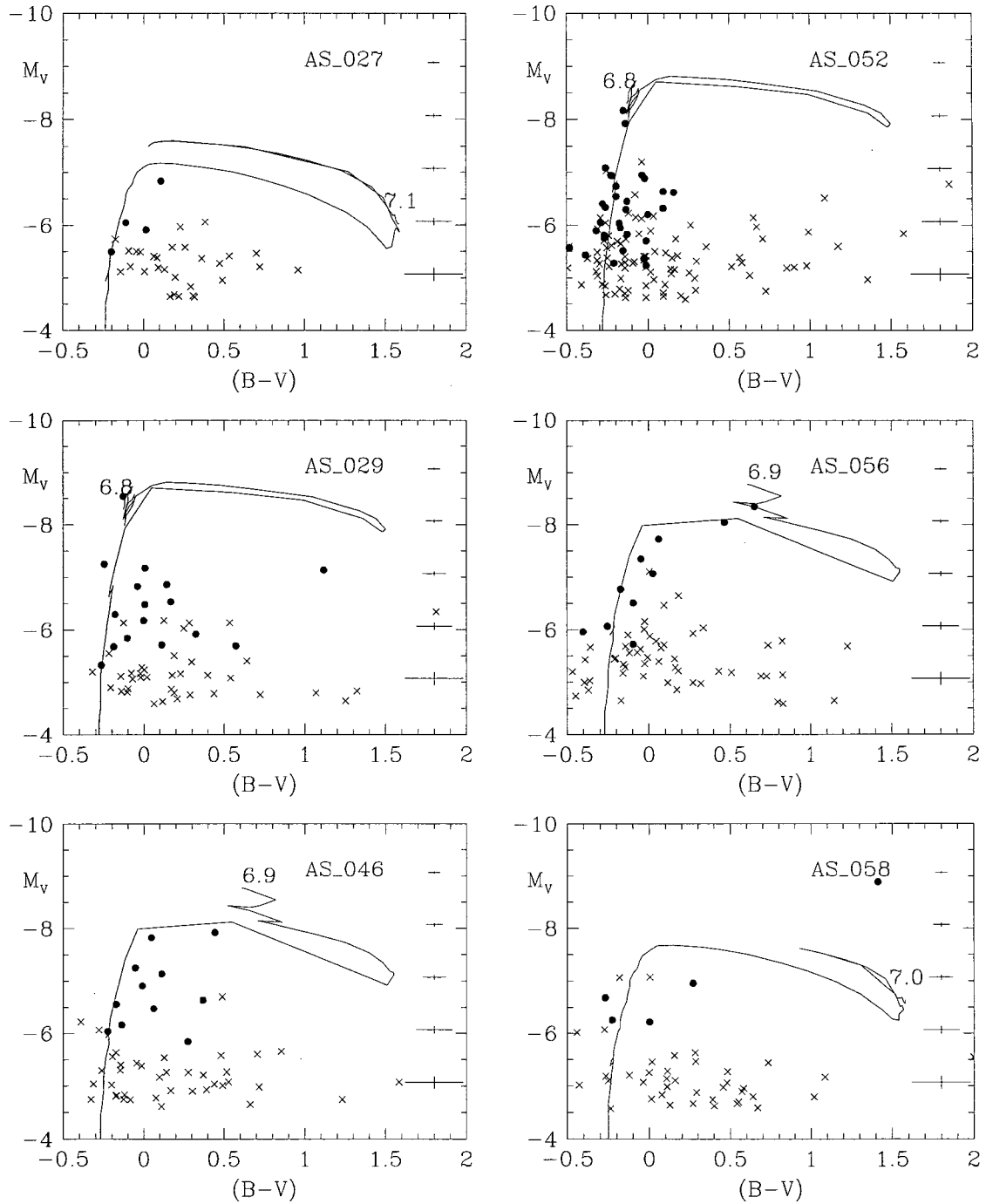
Fig. 5.— Continued.
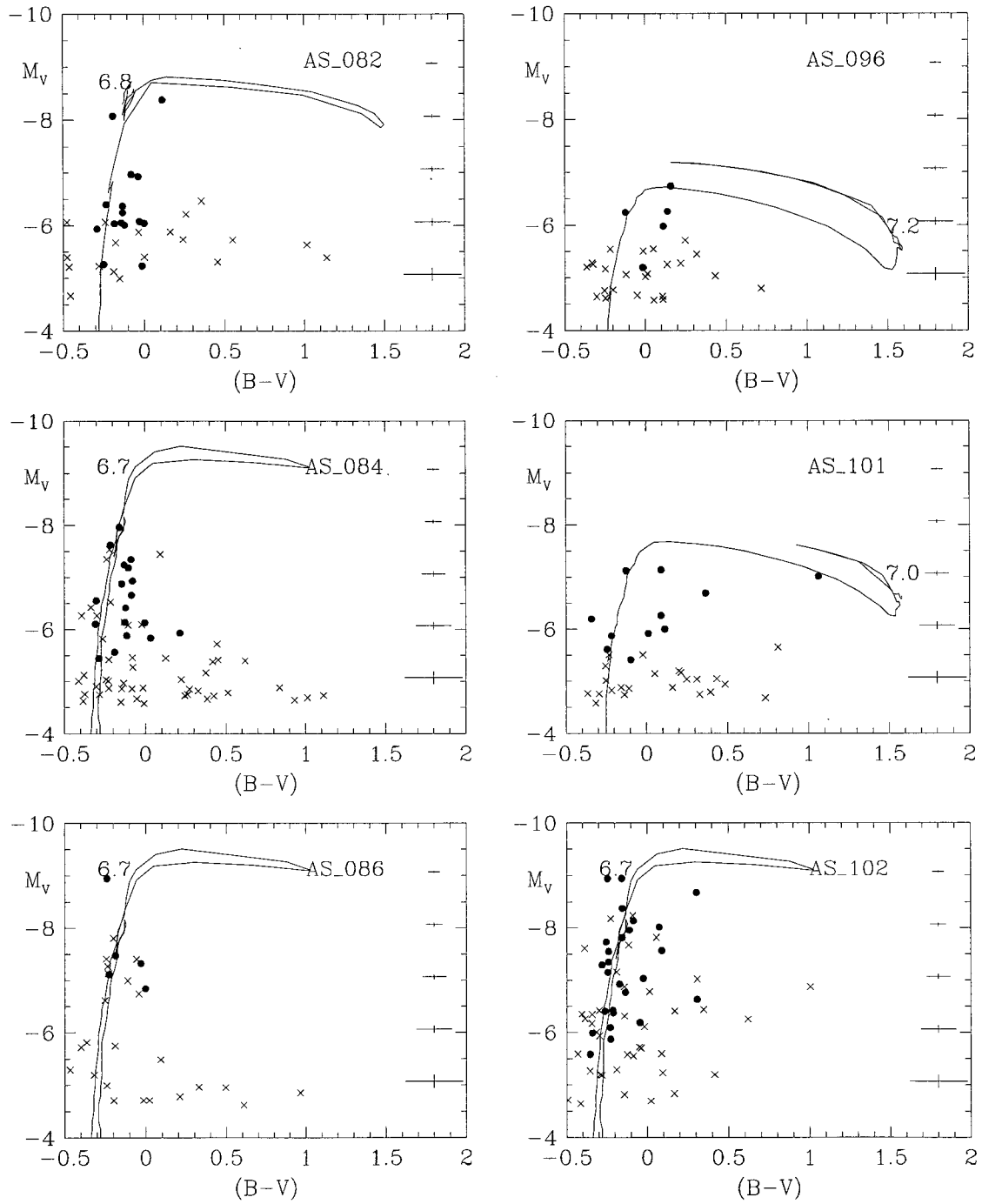
Fig. 5.— Continued.

IV. GLOBULAR CLUSTER CANDIDATES

(a) Search Method

Globular clusters in NGC 300 are barely resolved in our images. We have used photometric information, morphological parameters and visual inspection to survey globular cluster candidates as follows. From the $(V, B-V)$ CMD in Fig. 3, we have first taken the point sources with $V < 20.0$ mag and $0.3 < (B - V) < 2.0$ to search for globular cluster candidates. We have considered $V = 20.0$ mag as the reliable magnitude limit and $0.3 < (B - V) < 2.0$ to be the safe color range that contains all the GC candidates in NGC 300. For these selected point sources we have calculated the morphological image classification parameters (r_1 and r_{-2} radial moments) in three (V-band and two I-band) best seeing images. The two radial moments are effective image radii in pixel units, where r_1 is an indicator of image wing spread and r_{-2} indicates the image central concentration (see Harris et al. 1991; Kim et al. 2002; Lee et al. 2002). Because the images have degradations at the corners, we only considered the objects inside of a circle centered at the image center and with the diameter of the image width ($20.'5$).

Fig. 6 shows the r_1 and r_{-2} parameters calculated on the V-band image. The horizontal sequence of objects are mainly stars, objects with a little larger moment values should be GCs in NGC 300, and some objects with largest moment values are probably background galaxies. The box region contains the objects for which we have performed visual examination on each image and investigated radial, contour, and surface profiles. The circled objects denote the resulting GC candidates and the size of the circle is proportional to the probability to be a GC; the largest circles denote probable GC candidates (class 1), the intermediate size circles denote the possible candidates (class 2), and the smallest circles denote doubtful candidates (class 3).

Fig. 7 shows the V-band mosaic images and radial profiles of a typical star and a class 1 GC candidate discovered in this study. The FWHM of the star in Fig. 7 is ~ 2.4 pixel, while that of the GC candidate is ~ 2.8 pixel. Though the GC candidate is fainter than the star (V=18.2 versus V=17.4), it is clear that the GC candidate is more extended than the star.

We also have performed smoothing the images using the IRAF/RMEDIAN package and subtracted the results from the originals to form the final images on which the GC search was made again. While these images clearly show the fine structures of NGC 300 especially in the nuclear region and patchy regions, they are not much better in the search for GCs than the original images.

There are several sources that we could not be able to investigate the image structure due to the crowding of two or more objects in small region and large pixel size of our images (1 px = $0.''602 = 5.89$ pc assuming d $'= 2.02$ Mpc, and so $1'' = 9.79$ pc). Imaing data of
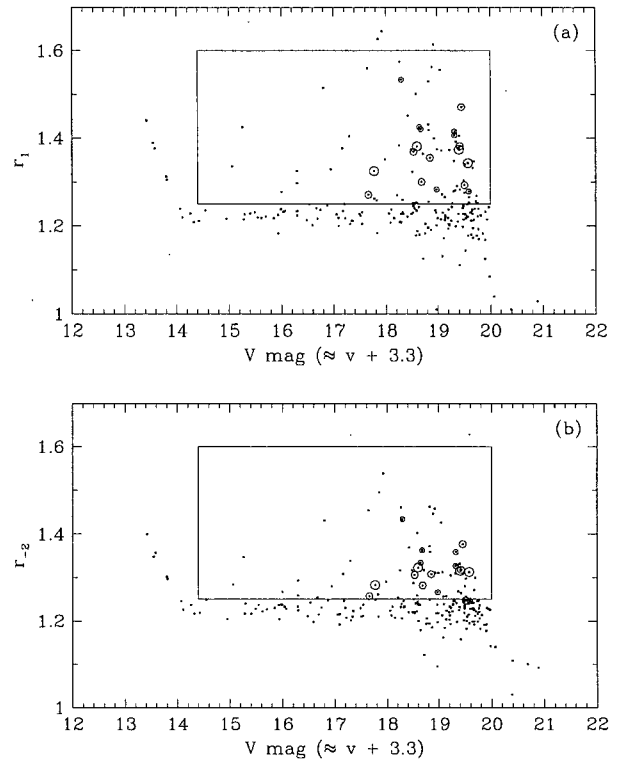
Fig. 6.— The distribution of morphological image classification parameters ((a) r_1 and (b) r_{-2}) calculated on the V-band image are plotted over the V magnitude. All objects with $V < 20$ and $0.3 < B - V < 2.0$ are plotted (N=223). The horizontal sequence of objects are mainly stars, while GCs in NGC 300 have a little larger moment values. Some objects with largest moment values are probably background galaxies. The objects in the box region are visually examined on the image and the circled objects denote the resulting GC candidates. The larger the circle, the higher the probability to be a GC.

better quality (e.g. Bright & Olsen 2000) will be helpful to uncover the nature of these objects.

(b) Search Result

In Table 4 we present the newly discovered GC candidates in NGC 300. Column 1 gives the GC candidate ID numbers. Columns 2 and 3 are the RA and DEC coordinates (epoch J2000), columns 4-7 are V magnitude, and $V - I$, $B - V$, and $U - B$ colors, respectively, columns 8-11 are the errors in V, $V - I$, $B - V$ and $U - B$, respectively, columns 12-15 are the number of independent measurements and the last column is the class of the candidates.

The positions of these GC candidates in the CMD and $(U - B, B - V)$ diagram are shown in Fig. 3 and Fig. 4, respectively. The V magnitudes of most of the candidates are between $\sim$18 to 20 mag. The $B - V$
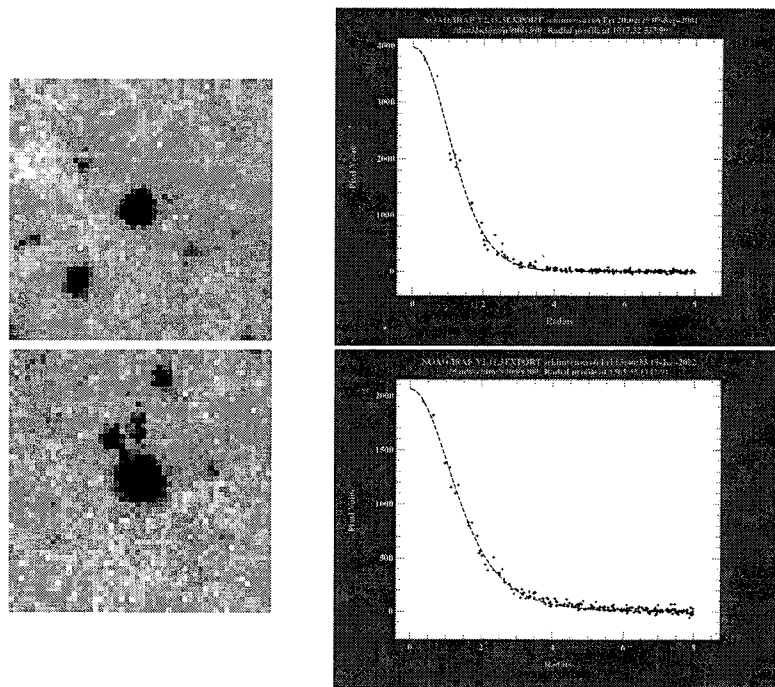
Fig. 7.— V-band mosaic images (30.″1 × 30.″1) and radial profiles of a typical star (upper panels, Table 2 ID=47, V=17.398, $B - V$=0.576) and a class 1 GC candidate (lower panels, GC candidate ID=12, Table 2 ID=72, V=18.158, $B - V$=0.601). North is to the down, and east is to the right on the images. The typical FWHM of stars in the V image is ∼ 2.4 pixel, while the FWHM of this GC candidate is ∼ 2.8 pixel.

colors of the candidates are between 0.3 and 1.1 and the $V - I$ are between 0.6 and 1.2. Some characteristics of these GC candidates will be discussed in the next Section.

V. DISCUSSION

(a) Stellar Mass Function

The upper part of stellar mass function (MF) of NGC 300 can be derived from the photometry of bright stars in the galaxy. But as mentioned in Section III (b) the most massive part of MF is highly uncertain because we have only the photometric data for the stars. Due to the degeneracy of $B - V$ color for the hottest stars (T_{eff} >20,000K), it is nearly impossible to estimate accurately the mass of blue stars in NGC 300. To show this effect more clearly, we plotted two CMDs with theoretical evolution tracks in Fig. 8. The evolution tracks in Fig. 8 (a) are those of the Padova group (Bertelli et al. 1994), and are transformed to the observational plane using the calibration of Sung (1995). The model shows that most massive star (m = $100 M_{\odot}$) does not evolve to the brightest part of the CMD. On the other hand, that of the Geneva group (Schaller et al. 1992) shows that 120 $M_{\odot}$ star evolves to the brightest part of CMD. The η Car, the most massive star in the Galaxy (m ≈ $100 M_{\odot}$) is one of the brightest stars in the Galaxy. This means that at least a few of the bright blue stars in NGC 300 have masses around $100 M_{\odot}$.

To derive the MF of NGC 300, we should know the mass - luminosity (ML) relation. To derive the ML relation, we used the evolution tracks by the Geneva group (Schaller et al. 1992) and the Padova group (Bertelli et al. 1994), and the calibration of Sung (1995). We simply divide the stars in the CMD into 4 groups (4 color bins - I: $B - V \leq 0.2$, II: $0.2 < B - V \leq 0.8$, III: $0.8 < B - V \leq 1.3$, and IV: $B - V > 1.3$). And we calculated the mean M_V for a given model star in each color bin, i.e. $< M_V > \equiv \int M_V(j) d\tau(j) / \int d\tau(j)$ during the star evolves in the given color bin. The ML relation derived from the above scheme is strongly dependent on the absolute magnitude which the star spends most of time for the given color bin, i.e. for the color bin II, III, and IV the position of helium burning phase. The theoretical ML relation for given color bin is presented in Fig. 9 (a). For the blue stars (group I), they are actually evolved blue stars, but the theoretical ML relation derived using the above scheme is that for main sequence (MS) stars, not for evolved blue (super)giants because the star of a given mass spends most of their life time in the MS stage. Therefore the theoretical ML relation for group I is inadequate for the actual case. For group I stars, we simply determined the mid-point of evolution tracks. The adopted ML relation for the group I is also presented in Fig. 9 (a).

To derive the luminosity function (LF) of each group, we calculated the number of stars for each group. And we subtracted the number of GC candidates and the

Table 4. GC candidates

ID	α (J2000)	δ (J2000)	V	$V-I$	$B-V$	$U-B$	ϵ_V	ϵ_{V-I}	ϵ_{B-V}	ϵ_{U-B}	n_{obs}				class
1	0:54:22.07	-37:43:22.1	19.634	1.288	1.231	0.192	0.066	0.091	0.096	0.171	1	1	1	1	1
2	0:54:35.80	-37:43:05.6	17.878	0.769	0.561	-0.156	0.034	0.046	0.056	0.055	1	1	1	1	2
3	0:54:40.02	-37:49:18.5	19.571	0.868	0.720	-0.092	0.086	0.142	0.117	0.117	1	1	1	1	3
4	0:54:45.62	-37:43:41.0	18.839	0.973	0.755	0.197	0.044	0.064	0.059	0.084	1	1	1	1	2
5	0:54:49.35	-37:43:30.5	19.076	0.786	0.621	0.191	0.056	0.085	0.071	0.093	1	1	1	1	2
6	0:54:51.67	-37:39:38.0	19.073	$\cdots$	0.444	-2.349	0.167	$\cdots$	0.228	0.178	1	0	1	1	3
7	0:54:53.22	-37:43:11.1	19.213	1.639	0.765	-0.080	0.164	0.176	0.192	0.130	1	1	1	1	1
8	0:54:57.41	-37:33:55.3	18.705	1.173	1.116	0.348	0.077	0.101	0.101	0.113	1	1	1	1	2
9	0:54:57.57	-37:36:37.0	19.728	1.552	0.665	-0.409	0.043	0.053	0.064	0.132	1	1	1	1	2
10	0:54:59.03	-37:36:24.4	19.188	0.557	0.380	-0.244	0.048	0.068	0.056	0.055	1	1	1	1	3
11	0:55:01.44	-37:37:21.8	19.739	0.955	0.714	0.172	0.078	0.118	0.096	0.152	1	1	1	1	1
12	0:55:11.03	-37:36:46.1	18.158	1.308	0.601	0.321	0.108	0.122	0.119	0.074	1	1	1	1	1
13	0:55:11.17	-37:33:13.9	19.537	0.724	0.609	-0.151	0.090	0.141	0.122	0.115	1	1	1	1	3
14	0:55:17.67	-37:36:57.9	19.831	1.166	1.094	0.174	0.091	0.137	0.144	0.206	1	1	1	1	2
15	0:55:21.81	-37:45:40.1	19.625	0.608	0.423	0.089	0.073	0.125	0.100	0.117	1	1	i	1	2
16	0:55:27.56	-37:46:09.4	18.905	1.213	1.065	0.723	0.085	0.136	0.123	0.178	1	1	1	1	3
17	0:55:38.79	-37:46:30.7	18.884	1.206	1.074	0.267	0.091	0.137	0.122	0.133	1	1	1	1	3
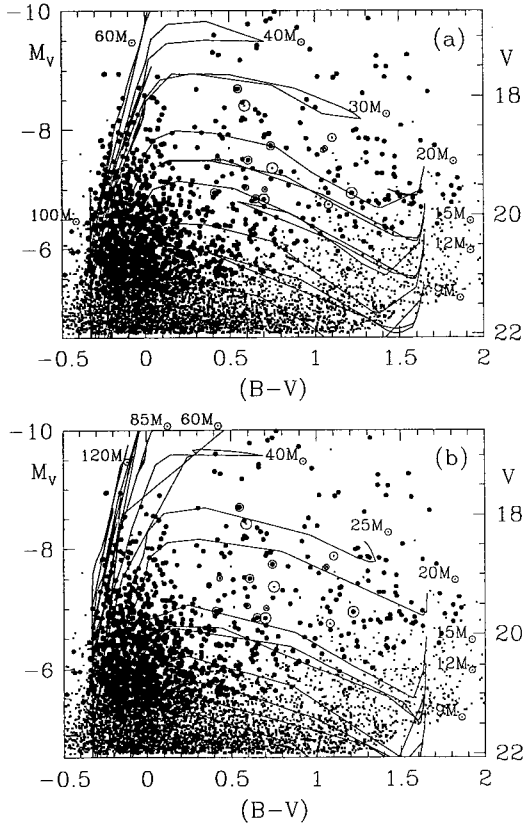
Fig. 8.— Observation HR Diagram of NGC 300. (a) The $(M_V, B-V)$ diagram. The superimposed evolution tracks from Bertelli et al. (1994) are for a metallicity of $Z = 0.02$. The transformation to the observational plane was performed using the calibration of Sung (1995). (b) The same as (a), but the superimposed evolution tracks are from Schaller et al. (1992). All the symbols are the same as in Fig. 3.

number of foreground stars based on the estimates by Ratnatunga & Bahcall (1985) for the Sculptor dwarf galaxy. Ratnatunga & Bahcall (1985) presented the expected number of foreground stars in the direction of the Sculptor dwarf galaxy in $\Delta V = 2$ mag and three bins in $B-V$ (< 0.8, $0.8 - 1.3$, and > 1.3 mag). We estimated the number of stars for given color bin by keeping the trend of the variation of star number. For blue stars (group I) most of them are bona fide members of NGC 300. Even though there are apparently many bright stars in the group II (see Fig. 8), the final number of stars in group II is very few. The resulting LF of stars in NGC 300 is presented in Fig. 9 (b). In the transformation of the LF to the MF, we used the ML relations derived above using the models by the Geneva group, i.e. $\xi(\log m) d\log m \equiv N(M_V) dM_V$ (Salpeter 1955). The resulting MF of each group is presented in Fig. 9 (c).

To derive the initial mass function (IMF) of a heterogeneous group of stars, such as a galaxy like NGC 300, we should know the star formation history. It is practically impossible to know the history of star formation in NGC 300. To derive the IMF of NGC 300, we assumed that the star formation rate is constant with time. This assumption is valid at least for the massive stars. For this case, the transformation of MF to IMF is very simple, i.e. only applying the difference in the total life span between stars with different masses. By interpolating the MF of each group, we derived the MF of bright stars in NGC 300 by summing up the MF of each group. After that by dividing the difference in life span, we derived the IMF of NGC 300. The total MF and IMF is presented in the same figure. The slope of IMF ($\Gamma \equiv d\log\xi(\log m)/d\log m$) of NGC 300 is -2.6 ± 0.3. This value is steeper than that of the solar neighborhood ($\Gamma = -1.35$: Salpeter 1955), but less steeper than the general field of the magellanic clouds ($\Gamma = -4.1 \pm 0.2$ for LMC and -3.7 ± 0.5 for SMC: Massey et al. 1995). The IMF for NGC 300 is that for the

bright stars measured in this study, i.e. a mixed group of stars, and the slope of the IMF is reasonably agreed to the result obtained by Massey et al. (1995). In addition, if the star formation rate is a decreasing function of time, then the resulting slope of IMF is steeper than the actual value of the slope.

(b) The Brightest Stars

The birghtest stars in galaxies have been used as distance indicator (Lyo & Lee 1997). In order to avoid the contamination of foreground stars, the mean brightness of three brightest stars in a galaxy is used for this purpose. For NGC 300, the identification of red supergiant stars is very difficult due to the possible contamination of foreground thick disk or halo stars in the Galaxy as well as the GCs in NGC 300. For blue stars in NGC 300, they are well-separated from the foreground stars, and therefore they are nearly free from the contamination.

Three brightest blue stars in NGC 300 are easily selected: # 50, 51, and 52 with similar magnitudes. The mean magnitude and color of these stars are derived to be $< V > = 17.62 \pm 0.01$ mag, $< B - V > = -0.21 \pm 0.05$ mag. Assuming the distance to NGC 300 adopted in this study, the mean absolute magnitude of three brightest blue stars is derived to be $< M_V^{BSG}(3) > = -8.95$ mag. The brightness of these blue supergiants in NGC 300 is very similar to that of three blue supergiants in M33 (Lyo & Lee 1997). The calibration for the blue supergiants was given by Lyo & Lee (1997): $< M_V^{BSG}(3) > = 0.32(\pm 0.05)M_B^T - 2.69(\pm 0.94)$. Using this calibration, the absolute magnitude of the brightest blue supergiants expected for the luminosity of NGC 300 ($M_B^T = -18.59$) is derived to be $< M_V^{BSG}(3) > = -8.63(\pm 0.54)$, which agrees within calibration uncertainty with the value obtained in this study.

(c) Characteristics of the Globular Cluster Candidates

i) Luminosity function

Fig. 10 shows the GC luminosity function (GCLF) of NGC 300 obtained for the 17 GC candidates found in Section IV relative to the GCLF of M31 GCs. Only class 1 objects are plotted in Fig. 10 (a), objects of classes of 1 and 2 are plotted in Fig. 10 (b), and objects of all three classes are plotted in Fig. 10 (c). Milky Way Galaxy (MWG) GC data (N=146) taken from Harris (1996) are shown in dotted lines and M31 GC data (N=429) taken from Barmby et al. (2000) are also shown in dashed lines for comparison.

GCLF is well fitted by Gaussin or t_5 function (Barmby, Huchra, & Brodie 2001; Secker 1992; Secker & Harris 1993). However our GCLF of NGC 300 shown in Fig. 10 (c) is far from Gaussin shape and clearly lacks symmetry. Considering the fact that the faintest bin of our GCLF is much affected by the photometric errors and

Fig. 9.— The luminosity and mass function of the bright stars in NGC 300. (a) The mass - luminosity relation for each group. Open and filled symbols represent, respectively, the relation from Bertelli et al. (1994) and Schaller et al. (1992). The circle, diamond, triangle, and square denote, respectively, the theoretical mass - luminosity relations for group I, II, III, and IV. The circle with dot represents the adopted relation for group I (blue stars). See text for more details. (b) The luminosity function. The contribution of foreground field stars were subtracted using the model calculation by Ratnatunga & Bahcall (1985). (c) The mass function of NGC 300. The mass function of each group was derived from the luminosity function obtained in (b) using the mass - luminosity relation in (a). The open circle and star mark represents, respectively, the total mass function and the initial mass function of NGC 300. See text for the derivation of the initial mass function.

Fig. 10.— Luminosity function of the GC candidates in NGC 300 (solid lines). Data for the MWG GCs (Harris 1996; dotted lines) and M31 GCs (Barmby et al. 2000; dashed lines) are also plotted for comparison.

assuming the turnover of NGC 300 GCLF is also at $M_V \sim -7.4$ as in the case of the Milky Way (Harris 2001), it can be said that we have obtained the bright half of the LF.

From the largest number GCLF of NGC 300 (Fig. 10 (c)) it is concluded that the faintest bin of GCLF of NGC 300 may possibly contain some non-GCs, and there maybe more fainter (than the turnover) GCs not discovered yet in NGC 300. Further search for the rest of GCs is needed for this galaxy.

ii) Color distribution

We present the $B - V$ and $V - I$ color distribution of our GC candidates in Fig. 11. The data of MWG GCs (Harris 1996; N=117 for $B - V$ and N=97 for $V - I$) and M31 GCs (Barmby et al. 2000; N=383 for $B - V$ and N=242 for $V - I$) are also plotted with dotted and dashed lines, respectively. The labels in the ordinates are for the GC candidates in NGC 300 and are in arbitrary scales for the GCs in M31 and MWG.

In general the color distributions of the three galaxies agree well, though there are some differences: (1) the peak is skewed to the blue side ($(B-V)_{peak} \sim 0.5$) in the $(B - V)$ color distribution (Fig. 11 (c)) and there are double peaks ($(V - I)_{peak} \sim 0.6$ and 1.2) in the $(V - I)$ color distribution (Fig. 11 (f)), and (2) there are more blue GC candidates in NGC 300 than red GC candidates compared to MWG or M31. The reason for the latter might be either (i) NGC 300 has actually larger rate of blue to red clusters than MWG or M31 or (ii) we have discarded more red GC candidates than blue ones taking them to be background galaxies or foreground stars during the search process. It is not easy to find out which is the cause at the present. It is needed to perform a new, deep search for GCs in NGC 300 to find more clusters and to distinguish which is the cause.

iii) Spatial distribution

In Fig. 12 we show the histogram of the projected galactocentric distances of the GC candidates from the nuclces of NGC 300 in arcmin. Most candidates distribute evenly in the range $1' < R_{gc} < 11'$, while there are more objects at $4' < R_{gc} < 8'$. It is not clear if this underabundance of GC candidates in the galaxy center is real or due to the low discovery rate of our search in the galactic center region.

(d)   Nucleus

The nucleus of NGC 300 was originally included in our GC candidates as Class 1 or 2 object, which means it could be regarded as a star cluster in photometric images. Based on little emission from ionized gas from the nuclear region of NGC 300, Soffner et al. (1996) have suggested that the nucleus of NGC 300 is very probably an unresolved compact stellar cluster, similar to the nucleus of M33 (Kormendy & McClure 1993). A
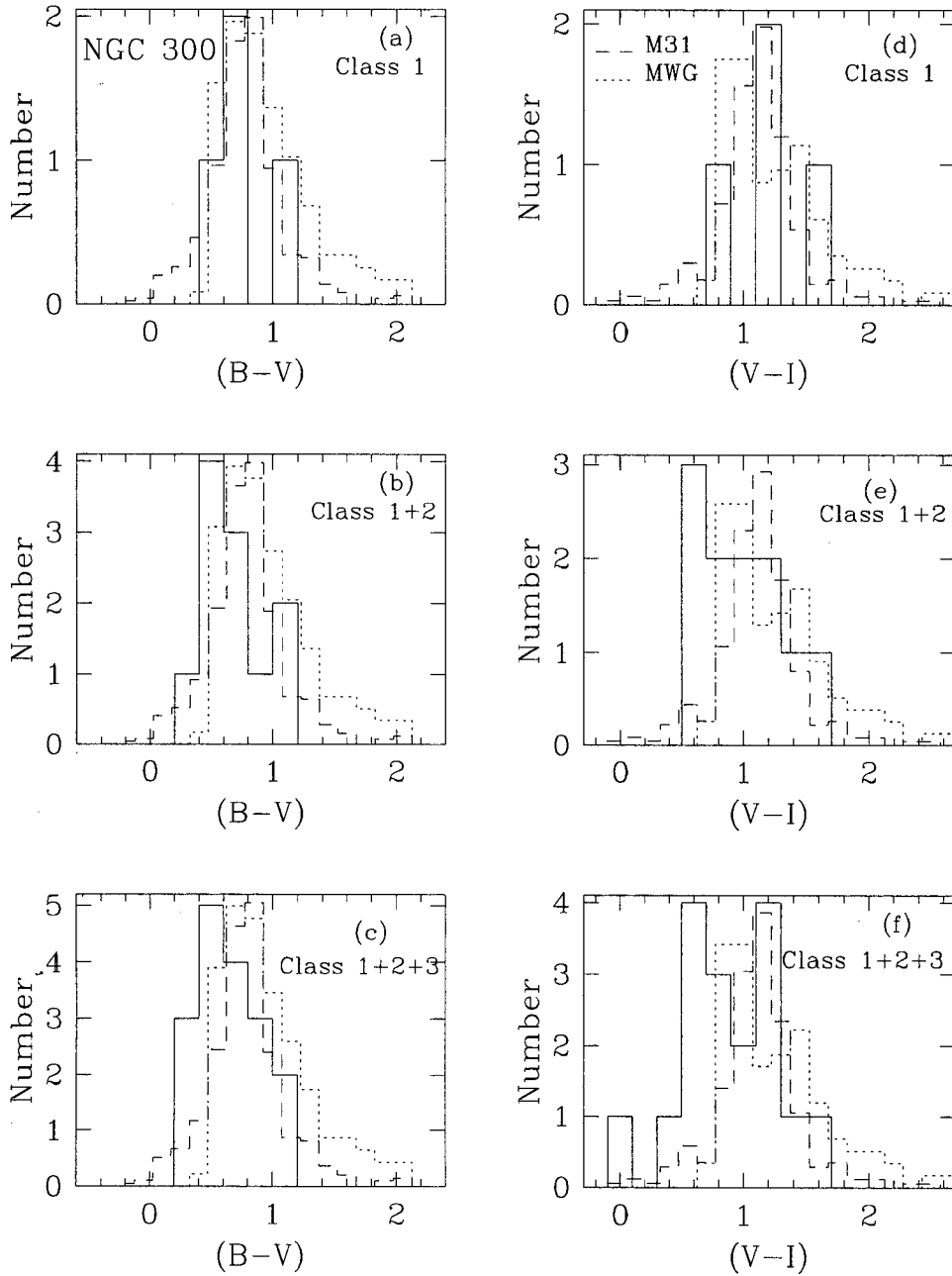
Fig. 11.— Color distribution of the GC candidates in NGC 300 (solid lines). Data for the MWG GCs (Harris 1996; dotted lines) and M31 GCs (Barmby et al. 2000; dashed lines) are also plotted for comparison. The labels in the ordinates are for the GC candidates in NGC 300 and are in arbitrary scales for the GCs in M31 and MWG.
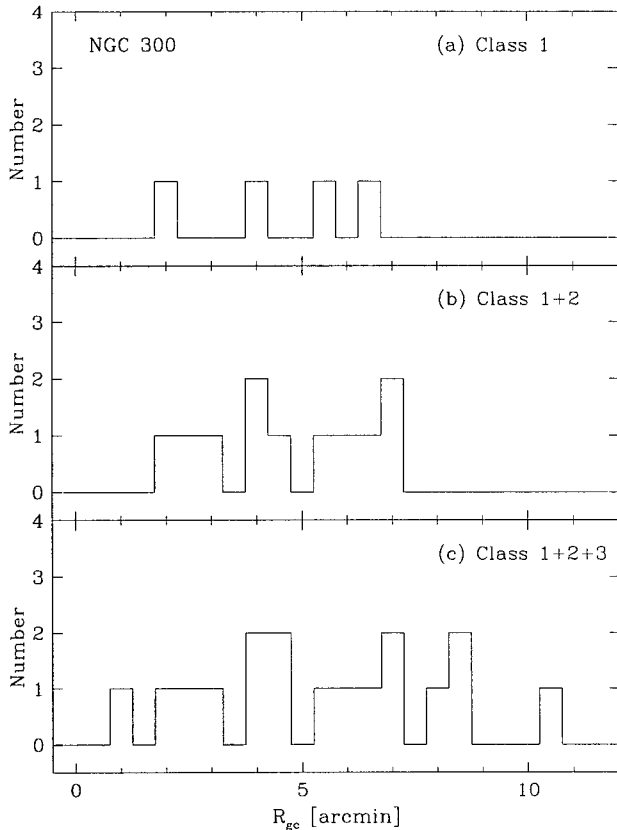
Fig. 12.— Histogram of the projected galactocentric distances of the GC candidates from the nuclues of NGC 300.

detailed aperture photometry and surface photometry of the nucleus region and the surface photometry of the whole CCD area of NGC 300 (just like in the case of NGC 205: Kim & Lee 1998) will follow in a subsequent paper(Kim et al. in preparation).

VI.   SUMMARY AND CONCLUSIONS

We have presented the $UBVI$ CCD photometry of $20.'5 \times 20.'5$ area of the Sculptor group galaxy NGC 300. The primary results from this study of the stellar populations and the GC candidates in this galaxy are summarized as follows.

(1) The $(V, B - V)$ CMD shows well-defined blue stars extending up to $V \approx 17.5$ mag.

(2) The $(U - B, B - V)$ diagram shows that most bright blue stars in NGC 300 are blue supergiants.

(3) CMDs of 18 OB associations with more than 30 member stars are presented together with ages from the Padova isochrones.

(4) The initial mass function (IMF) of bright stars in NGC 300 is derived to have the slope of $\Gamma = -2.6 \pm 0.3$, which is steeper than that of the solar neighborhood ($\Gamma = -1.35$), but less steeper than those of the general

field of the magellanic clouds ($\Gamma = -4.1$ for LMC and -3.7 for SMC).

(5) Assuming the distance of NGC 300 to be $(m - M)_0 = 26.53 \pm 0.07$, the mean absolute magnitude of three brightest blue stars is estimated to be $< M_V^{BSG}(3) > = -8.95$ mag.

(6) From the search for GCs in NGC 300, we discovered 17 GC candidates and they are 4 probable (class 1), 7 possible (class 2), and 6 doubtful (class 3) candidates. Some characteristics of these newly found GC candidates are discussed.

REFERENCES

Barmby, P., Huchra, J. P., Brodie, J. P., Forbes, D. A., Schroder, L. L., & Grillmair, C. J. 2000, M31 globular clusters: colors and metallicities, AJ, 199, 727

Barmby, P., Huchra, J. P., & Brodie, J. P. 2001, AJ, The M31 globular cluster luminosity function, AJ, 121, 1482

Beasley, M. A., & Sharples, R. M. 2000, Spectroscopy of globular cluster candidates in the Sculptor group galaxies NGC 253 and 55, MNRAS, 311, 673

Bertelli, G., Bressan, A., Chiosi, C., Fagotto, F., & Nasi, E. 1994, Theoretical isochrones from models with new radiative opacities, A&AS, 106, 275

Blair, W. P., & Long, K. S. 1997, Identification of supernova remnants in the Sculptor group galaxies NGC 300 and NGC 7793, ApJS, 108, 261

Blecha, A. 1986, Search for the globular clusters in nearby galaxies. I. NGC 253, A&A, 154, 321

Breysacher, J., Azzopardi, M., Testor, G., & Muratorio, G. 1997, Wolf-Rayet stars detected in 5 associations of NGC 300, A&A, 326, 976

Bright, J., & Olsen, K. 2000, Identifying the globular cluster systems of the Sculptor Group, BAAS, 196, 2805

Carignan, C., 1985, Surface photometry of the Sculptor group galaxies: NGC 7793, NGC 247, and NGC 300, ApJS, 58, 107

Côté, S., Freeman, K. C.; Carignan, C., & Quinn, P. J. 1997, Discovery of numerous dwarf galaxies in the two nearest groups of galaxies, AJ, 114, 1313

Da Costa, G. S., & Graham, J. A. 1982, Globular clusters in the Sculptor group galaxy NGC 55, ApJ, 261, 70

Davidge, T. J. 1998, The evolved red stellar contents of the Sculptor group galaxies NGC 55, NGC 300, and NGC 7793, ApJ, 497, 650

de Vaucouleurs, G., de Vaucouleurs, A., Corwin, H. G., Jr., Buta, R. J., Paturel, G., & Fouqué, P. 1991, Third Reference Catalogue of Bright Galaxies (New York: Springer-Verlag) (RC3)

Freedman, W. L., Madore, B. F., Hawley, S. L., Horowitz, I. K., Mould, J., Navarrete, M., & Sallmen, S. 1992, New Cepheid distances to nearby galaxies based on $BVRI$ CCD photometry. III - NGC 300, ApJ, 396, 80

Freedman, W. L., et al. 2001, Final results from the *Hubble Space Telescope* Key Project to measure the Hubble Constant, ApJ, 553, 47

Graham, J. A. 1981, A photoelectric *UBVRI* sequence near NGC 300 for the calibration of faint stellar magnitudes, PASP, 93, 29

Graham, J. A. 1984, The Cepheid variables in NGC 300, AJ, 89, 1332

Harris, W. E. 1996, A catalog of parameters for globular clusters in the Milky Way, AJ, 112, 1487

Harris, W. E. 2001, Globular Cluster Systems, in Saas-Fee Advanced Course 28, Star Clusters, ed. L. Labhardt & B. Binggeli (New York: Springer-Verlag), 285

Harris, W. E., Allwright, J. W. B., Pritchet, C. J., & van den Bergh, S. 1991, The luminosity distribution of globular clusters in three giant Virgo ellipticals, ApJS, 76, 115

Jerjen, H., & Rejkuba, M. 2001, Tip of the red giant branch distance for the Sculptor group dwarf ESO 540-032, A&A, 371, 487

Kilkenny, D., van Wyk, F., Roberts, G., Marang, F., & Coper, D. 1998, Supplementary southern standards for *UBV(RI)$_C$* photometry, MNRAS, 294, 93

Kim, S. C. & Lee, M. G. 1998, Surface photometry of the dwarf elliptical galaxies NGC 185 and NGC 205, JKAS, 31, 51

Kim, S. C., Lee, M. G., Geisler, D., Seguel, J., Sarajedini, A., & Harris, W. E. 2002, Washington photometry of new globular clusters in M31, in IAU Symp. 207, Extragalactic Star Clusters, ed. E. K. Grebel, D. Geisler, & D. Minniti, in press (astro-ph/0109217)

Kormendy, J., & McClure, R. D. 1993, The nucleus of M33, AJ, 105, 1793

Lee, M. G., Kim, S. C., Geisler, D., Seguel, J., Sarajedini, A., & Harris, W. E. 2002, New CCD survey of globular clusters in M31, in IAU Symp. 207, Extragalactic Star Clusters, ed. E. K. Grebel, D. Geisler, & D. Minniti, in press (astro-ph/0109219)

Liller, W., & Alcaino, G. 1983a, A search for globular clusters around the edge-on spiral galaxy NGC 55, ApJ, 264, 53

Liller, W., & Alcaino, G. 1983b, A search for globular clusters around the edge-on late-type spiral galaxy NGC 253, ApJ, 265, 166

Lyo, A.-R., & Lee, M. G. 1997, The brightest stars in galaxies as distance indicators, JKAS, 30, 27

Massey, P., Lang, C. C., DeGioia-Eastwood, K., & Garmany, C. D. 1995, Massive stars in the field and associations of the magellanic clouds: The upper mass limit, the initial mass function, and a critical test of main-sequence stellar evolutionary theory, ApJ, 438, 188

Menzies, J., Marang, F., Laing, J. D., Coulson, I. M., & Engelbrecht, C. A. 1991, *UBV(RI)$_C$* photometry of equatorial standard stars - A direct comparison between the northern and southern systems, MNRAS, 248, 642

Pannuti, T. G., Duric, N., Lacey, C. K., Goss, W. M., Hoopes, C. G., Walterbos, R. A. M., & Magnor, M. A. 2000, An X-ray, optical, and radio search for supernova remnants in the nearby Sculptor group Sd Galaxy NGC 300, ApJ, 544, 780

Pietrzyński, G., Gieren, W., Fouqué, P., & Pont, F. 2001, A catalog of OB associations in the spiral galaxy NGC 300, A&A, 371, 497

Ratnatunga, K. U., & Bahcall, J. N. 1985, Estimated number of field stars toward Galactic globular clusters and Local Group galaxies, ApJS, 59, 63

Read, A. M., & Pietsch, W. 2001, X-ray emission from the Sculptor galaxy NGC 300, A&A, 373, 473

Read, A. M., Ponman, T. J., & Strickland, D. K. 1997, *ROSAT* PSPC observations of nearby spiral galaxies - I. The data, MNRAS, 286, 626

Richer, H. B., Pritchet, C. J., & Crabtree, D. R. 1985, Luminous late-type stars in NGC 300, ApJ, 298, 240

Rogstad, D. H., Crutcher, R. M., & Chu, K. 1979, Aperture-synthesis observations of H I in the galaxy NGC 300, ApJ, 229, 509

Salpeter, E. E. 1955, The luminosity function and stellar evolution, ApJ, 121, 161

Sandage, A. R., & Tammann, G. A. 1981, A Revised Shapley-Ames Catalog of Bright Galaxies (Washington, DC: Carnegie Institution)

Schaller, G., Schaerer, D., Meynet, G., & Maeder, A. 1992, New grids of stellar models from 0.8 to 120 solar masses at Z = 0.020 and Z = 0.001, A&AS, 96, 269

Schlegel, D., Finkbeiner, D., & Davis, M. 1998, Maps of dust infrared emission for use in estimation of reddening and Cosmic Microwave Background Radiation foregrounds, ApJ, 500, 525

Secker, J. 1992, A statistical investigation into the shape of the globular cluster luminosity distribution, AJ, 104, 1472

Secker, J., & Harris, W. E. 1993, A maximum likelihood analysis of globular cluster luminosity distributions in the Virgo ellipticals, AJ, 105, 1358

Soffner, T., Méndez, R. H., Jacoby, G. H., Ciardullo, R., Roth, M. M., & Kudritzki, R. P. 1996, Planetary nebulae and H II regions in NGC 300, A&A, 306, 9

Stetson, P. B. 1990, On the growth-curve method for calibrating stellar photometry with CCDs, PASP, 102, 932

Sung, H. 1995, The *UBV* CCD photometry of eight young open clusters, PhD thesis, Seoul National Univ.

Sung, H., Bessell, M. S., Lee, H.-W., Kang, Y. H., & Lee, S.-W. 1999, *UBVI* CCD photometry of M11 - II. New photometry and surface density profiles, MNRAS, 310, 982

Sung, H. & Bessell, M. S. 2000, Standard stars: CCD photometry, transformations and comparisons, PASA, 17, 244

van den Bergh, S. 1999, The nearest group of galaxies, ApJ, 517, L97

Walker, A. R. 1995, CCD Photometry of a sequence near NGC 300, PASP, 107, 683

Watson, A. M., et al. 1996, The discovery of young, luminous, compact stellar clusters in the starburst galaxy NGC 253, AJ, 112, 534

Whiting, A. B. 1999, Angular momentum in the Sculptor
    Group, AJ, 117, 202